Modelling changes in transmural propagation and susceptibility to arrhythmia induced by volatile anaesthetics in ventricular tissue

Henggui Zhang, Tao Tao, Sanjay Kharche, Simon M. Harrison

www.elsevier.com/locate/yjtbi

Modelling changes in transmural propagation and susceptibility to arrhythmia induced by volatile anaesthetics in ventricular tissue

Henggui Zhang, Tao Tao, Sanjay Kharche, Simon M. Harrison

PII: S0022-5193(08)00635-8
DOI: doi:10.1016/j.jtbi.2008.12.004
Reference: YJTBI5392

To appear in: *Journal of Theoretical Biology*

Received date: 21 July 2008
Revised date: 28 November 2008
Accepted date: 2 December 2008

Cite this article as: Henggui Zhang, Tao Tao, Sanjay Kharche and Simon M. Harrison, Modelling changes in transmural propagation and susceptibility to arrhythmia induced by volatile anaesthetics in ventricular tissue, *Journal of Theoretical Biology* (2008), doi:10.1016/j.jtbi.2008.12.004

Modelling changes in transmural propagation and susceptibility to arrhythmia induced by volatile anaesthetics in ventricular tissue

Henggui Zhang[a],Tao Tao[a], Sanjay Kharche[a], Simon M. Harrison[b].

[a]*Biological Physics Group, School of Physics & Astronomy, University of Manchester, UK*
and
[b]*Institute of Membrane and Systems Biology, Faculty of Biological Sciences, University of Leeds, UK*

***Address for Correspondence*:**

Dr. Simon M. Harrison, Institute of Membrane and Systems Biology,

Faculty of Biological Sciences, Garstang Building, University of Leeds, LS2 9JT, UK

Tel: 0113-343-4262, Fax: 0113-343-4262, E-mail: s.m.harrison@leeds.ac.uk

Running Head: Anaesthetic-induced arrhythmogenesis

Abstract:

Volatile anaesthetics such as halothane, isoflurane and sevoflurane inhibit membrane currents contributing to the ventricular action potential. Transmural variation in the extent of current blockade induces differential effects on action potential duration (APD) in the endocardium and epicardium which may be pro-arrhythmic. Biophysical modelling techniques were used to simulate the functional impact of anaesthetic-induced blockade of membrane currents on APD and effective refractory period (ERP) in rat endocardial and epicardial cell models. Additionally, the transmural conduction of excitation waves in 1-dimensional cell arrays, the tissue's vulnerability to arrhythmogenesis and dynamic behaviour of re-entrant excitation in 2-dimensional cell arrays were studied. Simulated anaesthetic exposure reduced APD and ERP in both epicardial and endocardial cell models. The reduction in APD was greater in endocardial than epicardial cells, reducing transmural APD dispersion consistent with experimental data. However, the transmural ERP dispersion was augmented. All three anaesthetics increased the width of the tissue's vulnerable window during which a premature stimulus could induce unidirectional conduction block but only halothane reduced the critical size of ventricular substrates necessary to initiate and sustain re-entrant excitation. All three anaesthetics accelerated the rate of re-entrant excitation waves, but only halothane prolonged the lifespan of re-entry. These data illustrate *in silico,* that modest changes in ion channel conductance abbreviate rat ventricular APD and ERP, reduce transmural APD dispersion, but augment transmural ERP dispersion. These changes collectively enhance the propensity for arrhythmia generation and provide a substrate for re-entry circuits with a longer half life than in control conditions.

Keywords: **A**rrhythmia; Action Potential, Halothane; Sevoflurane; Isoflurane

Introduction

Volatile general anaesthetics, such as halothane, isoflurane and sevoflurane are used worldwide to induce and maintain anaesthesia during surgery, however these agents have several unwanted side effects in cardiac tissue. These include effects on the strength of contraction of the heart as well as an impact on the electrical activity of heart tissue. Altered electrical behaviour, which results from anesthetic-induced blockade of ion channels can affect action potential configuration which may alter the propagation of electrical signals through the tissue and the propensity for induction or maintenance of arrhythmia.

In the clinical situation, use of volatile anaesthetics is associated with an increased incidence of ventricular arrhythmias (Atlee and Bosnjak, 1990, Blayney et al., 1999). As these agents have been reported to decrease the Ca^{2+} transient and contraction (Davies et al., 2000a), it is unlikely that such arrhythmias are secondary to a state of Ca^{2+} overload and are more likely due to altered electrical properties of the myocardium. Membrane currents which play an important role in determining the configuration of the ventricular action potential in rat myocardium include the L-type Ca^{2+} current (I_{Ca}) which contributes to the high plateau, the transient outward K^+ current (I_{to}) and the composite current, I_{ss}. I_{to} underlies the initial phase of repolarisation and is expressed to a greater degree in the ventricular sub-epicardium than sub-endocardium (Antzelevitch et al., 1991; Clark et al., 1993; Fedida and Giles, 1991, Nabauer et al., 1996; Volk et al., 1999; Wettwer et al., 1993) whereas other currents (e.g. I_{Ca}) are uniformly distributed across the ventricular wall. As a consequence of the greater expression of I_{to} in the sub-epicardium, repolarisation is accelerated and action potential duration (APD) shorter than in the sub-endocardium. This transmural gradient in APD contributes to the positive going T-wave of the electrocardiogram (ECG) and is important for normal repolarisation of the ventricle.

Halothane, isoflurane and sevoflurane have been reported to abbreviate ventricular APD at clinically relevant concentrations (Harrison et al., 1999; Hatakeyama et al., 1995; Hayes et al., 1996) which most likely results from the effect of these agents on membrane currents such as I_{Ca} (Bosnjak et al., 1991; Eskinder et al., 1991; Huneke et al., 2001; Ikemoto et al., 1985; Pancrazio, 1996; Rithalia et al., 2004; Terrar and Victory, 1988) and I_{to} (Davies et al., 2000b; Huneke et al., 2001; Rithalia et al., 2004). Recently, it has been reported (Rithalia et al., 2001; Rithalia et al., 2004) that halothane, isoflurane and sevoflurane reduced APD to a proportionately greater extent in the ventricular sub-endocardium than sub-epicardium, reducing the transmural gradient of APD. It was suggested that this reflected the greater inhibition of I_{to} by the anaesthetics in the sub-epicardium than sub-endocardium with the consequence that anaesthetic exposure had a greater impact on action potential configuration in sub-endocardial tissue (Rithalia et al., 2004). The transmural gradient in APD is important for the normal transmural dispersion of repolarization and refractoriness, which helps prevent re-entrant arrhythmias, and therefore factors that affect this gradient may be proarrhythmic.

The aim of this study was to use biophysical modelling to evaluate the functional impact of anaesthetic-induced changes in I_{Ca}, I_{to} and I_{ss} on the electrical properties of rat myocardium. Specifically we investigated whether experimentally-determined changes in these membrane currents could account for the changes in action potential configuration and the transmural heterogeneity in APD observed experimentally. In addition we investigated how such ionic and cellular changes influenced transmural dispersion in effective refractory period (ERP), ventricular conduction and susceptibility to arrhythmogenesis. To achieve this we constructed a multi-cellular strand model of 1-dimensional arrays of cells spanning the ventricular free wall, which incorporated both intercellular electrical coupling and the different electrical properties of cells from the endo- and epi-cardium. The model was used to simulate the actions of the three anaesthetics on the spread of electrical activity across the

wall. These strands were then combined to create a 2-dimensional transmural ventricular sheet model to investigate the vulnerability of the tissue to genesis and maintenance of re-entrant arrhythmias to further understand the arrhythmogenic nature of volatile anaesthetics.

Methods

Single cell model.

The rat ventricular cell model developed by Pandit et al. (2001) was chosen for this study because it includes recent advances in rat electrophysiology and reproduces the known transmural differences in APD of rat epicardial and endocardial cells. The equations and model parameters used are described in the Appendix. To simulate the effects of anaesthetic exposure on action potential configuration the maximal channel conductances of I_{Ca}, I_{to} and I_{ss} in the epicardial and endocardial cell models were modified to reflect the differences in channel conductance measured experimentally (Rithalia et al., 2004) in rat ventricular myocytes (see Table 1). To evoke an action potential, a series of supra-threshold stimuli with an amplitude 0.6 nA and duration of 5 ms was applied to the model at a frequency of 5 Hz (S1). The method described in our previous study (Salle et al., 2008) was used to analyse the characteristics of simulated action potentials. Hereafter APD_{90} denotes the duration of action potentials at 90% repolarisation. At the end of the stimulus sequence, a premature test stimulus (S2) with variable time intervals was applied. The effective refractory period (ERP) was measured as the smallest stimulus interval (SI) for which the overshoot of the S2-evoked AP reached 80% of that induced by the S1 stimulus (Workman et al., 2001).

One-dimensional (1D) transmural ventricle strand model.

A multi-cellular model of a 1D transmural strand of ventricular tissue was constructed using the diffusion partial differential equation:

$$\frac{\partial V_m}{\partial t} = -I_{tot} / C_m + \nabla \bullet (D \nabla V_m), \qquad \text{(Eq. 1)}$$

where C_m is the cell capacitance and I_{tot} is the total ionic current flowing across the cell membrane and is modelled as described by Pandit et al. (2001). In the model, heterogeneous electrical properties of cells were incorporated by varying the maximal ionic channel

conductance of various currents to reproduce the characteristics of endocardial and epicardial cells. D is the diffusion parameter describing the intercellular electrical coupling via gap junctions (Zhang and Hancox, 2004). In control simulations, D was set to a value of 1.13×10^{-2} mm^2 s^{-1} that gave a conduction velocity of a planar wave across the ventricular wall of 0.14 m s^{-1}, similar to the measured velocity in cultured rat ventricular tissue (Meiry et al., 2001). The impact of anaesthetics ($\leqslant$1 mM) on electrical coupling was simulated by reducing D from its control value of 1.13×10^{-2} mm^2 s^{-1} to 1.07×10^{-2} mm^2 s^{-1} (~5% reduction) for halothane, isoflurane and sevoflurane conditions (Burt and Spray, 1989). The 1D strand has a total length of 3 mm, of which 2 mm was designated as endocardial and 1 mm epicardial tissue. Due to the lack of detailed experimental data, the proportion of the two distinctive regions was chosen empirically such that a positive going T-wave in the computed pseudo ECG was generated in the control condition using the method described previously (Gima and Rudy, 2002). The simulated strand employed a spatial resolution of 0.1 mm – close to the length of single ventricular myocytes, which generated 20 nodes for the endocardial segment and 10 nodes for the epicardial segment. As the spatial resolution is close to the cell length of ventricular myocytes (80 – 150 μm), it is adequate for assumption of isopotentiality of a node of the model. Eq. 1 was numerically solved by the explicit Euler method with a time step of 0.1 μs. Numerical stability of the solutions was investigated by examining the influence of variation in time step (∂t, between 0.04 μs and 2.0 μs) and space step (∂X, from 0.05 to 0.1 mm) on measured conduction velocity of a solitary excitation wave propagating along the 1D tissue model. The computed conduction velocity was independent of variation in ∂t but there was a small increase of less than 7% when ∂X was decreased from 0.1 mm to 0.05 mm.

A 2D transmural ventricular tissue sheet was modelled by expanding the 1D transmural strand (length of 3 mm in the x direction) into a sheet with a width of 10 mm (in

the y direction). The spatial resolution in both x and y directions was the same as used in the 1D model.

Measurement of vulnerability to conduction block – temporal vulnerability.

The temporal vulnerability of cardiac tissue to re-entry was quantified by the width of a time window during which a test stimulus applied to the refractory tail of a previous excitation wave in the 1D tissue model (Eq. 1) evoked unidirectional conduction (Shaw and Rudy, 1995; Starmer et al., 1993; Zhang et al., 1998; Zhang and Holden, 1997). In cardiac tissue, a propagating action potential wavefront is followed by a refractory tail. A stimulus applied during this refractory tail can fail to excite the tissue (bidirectional block) but, after the tail, can induce a pair of action potentials (i.e. bidirectional conduction). During the tail there is a time window, the vulnerable window (VW), during which stimulation produces a solitary wave that propagates in the retrograde but not the anterograde direction (or, conversely, in the anterograde but not retrograde direction), resulting in unidirectional block. Such unidirectional block of conduction may lead to re-entry and the width of the VW of a tissue may therefore be used as an index for its vulnerability to re-entry (Shaw and Rudy, 1995; Starmer et al., 1993; Zhang et al., 1998; Zhang and Holden, 1997).

To measure the vulnerability of ventricular tissue, a standard S1-S2 stimulus protocol was used. A conditioning wave was initiated by supra-threshold stimuli (S1, with strength and durations as stated above for AP simulations) applied to a 0.3 mm segment at the endocardial end. A test stimulus (S2, with the same strength and duration as the one used for a conditioning wave, but 0.6 mm in spatial size) was applied at another point (1.0 mm away from the endocardial end of the strand) with a time delay Δt after the conditioning stimulus (S1). A unidirectional block falls in a time window (T1, T2), whose width (T2 –T1) provides

a measure of the vulnerability of the tissue to re-entry. This was measured for control and for the various simulated anaesthetic conditions.

Initiation of re-entry in a 2D tissue model.

Re-entry in a 2D tissue model was initiated by a similar standard S1-S2 protocol as used to measure vulnerability. The S1 was applied to the surface of the endocardial layer to evoke a planar excitation wave propagating towards the epicardial layer. During the vulnerable window, a S2 of variable intensity was applied to a local area of the tissue within the vulnerable window to evoke unidirectional propagation that can lead to re-entry. 2D simulations were run for 5 seconds, and the behaviours of spiral waves were quantified for the lifespan of re-entry, rate of re-entry and meandering path of the tips of re-entrant spiral waves.

Measurement of critical size of tissue to support re-entry – spatial vulnerability.

A S1-S2 protocol was also used to initiate spiral wave re-entry, however, here the S2 stimulus had variable spatial sizes (width 0.6 mm, length 3.0-8.0 mm) and was applied at a local epicardial region during the vulnerable time window of the local site. Each of the 2 ends of the S2-evoked excitation wave forms a tip of a pair of counter-rotating spiral waves. A large size of S2 is required to provide a sufficient re-entrant pathway of the two spiral arms, which is dependent on their wavelength. If the size of S2 is big enough, then the two spiral waves have sufficient circuit substrates and survive. Otherwise, the spiral wave pair collide and terminate. In order to evaluate the critical size of the re-entrant pathway of tissue, we estimated the minimal spatial length of S2 that supported the formation of re-entrant spiral waves under control conditions and those to simulate the presence of the volatile anaesthetics. The minimal length of S2 gives an alternative, inverse index of the susceptibility of tissue to re-entry- the larger the minimal length, the harder for the initiation of re-entry to occur.

Results

Halothane, isoflurane and sevoflurane on action potential configuration and ERP

Figure 1 illustrates action potential recordings from representative sub-endocardial and sub-epicardial left ventricular myocytes taken from a recent experimental study (Rithalia et al., 2004) under control conditions and with halothane (0.6 mM). APD_{90} was shorter in epicardial than endocardial cells (see Figure 1E for mean data) generating a transmural gradient of repolarisation. Figure 1B illustrates that halothane abbreviated both endocardial and epicardial APD with a greater proportionate effect evident in the endocardium. Consequently the transmural gradient of APD_{90} was reduced by halothane (see Fig 1E and F). Figure 1C and 1D illustrate action potentials generated by the mathematical model for endocardial and epicardial cells under control (Figure 1C) and halothane (Figure 1D) conditions. Under the control condition, the simulated endocardial and epicardial action potentials have similar configurations to the experimental recordings with APD_{90} values close to experimental data (Fig 1E). Alteration of membrane conductance of I_{Ca}, I_{to} and I_{ss} induced by halothane (Table 1), generated the simulated action potential waveforms in Figure 1D with APD_{90} values shown in Fig 1E. These data illustrate that the changes in these membrane currents can reproduce the actions of halothane on both the transmural action potential configuration and transmural APD as observed experimentally. We carried out a sensitivity analysis of the parameters altered in our simulation studies. Figure 1G illustrates the impact of a variety of altered ion conductances on APD_{90} and Figure 1H the resulting transmural difference in APD_{90} between endocardium and epicardium for each condition. These data illustrate that the transmural gradient of APD was most sensitive to changes in I_{Ca}.

The transmural gradient of APD_{90} for experimental data with halothane, isoflurane and sevoflurane were slightly reduced compared to simulated data although the overall trends

were similar; halothane induced the greatest reduction in the transmural gradient, followed by isoflurane with sevoflurane having the least effect.

Consistent with this, the three anaesthetics also decreased the measured ERP as shown in Figure 2. While halothane did not alter markedly the dispersion of ERP, isoflurane and sevoflurane both produced an inhomogeneous ERP reduction for the 2 different cell types, resulting in augmented transmural heterogeneity of ERP.

Temporal vulnerability to unidirectional conduction block

Simulations were then performed to determine whether or not the anaesthetics could be shown to generate an electrical substrate at the tissue level that would favour increased susceptibility to ventricular arrhythmia. Using 1D-tissue strand simulations, we quantified the temporal vulnerability of tissue to unidirectional conduction block in response to a test stimulus applied to the refractory tail of a previous excitation wave for control and each of the three anaesthetic conditions.

Figure 3 A-C shows the propagation of the conditioning excitation wave (spreading from endocardium to epicardium) and the response of the tissue to a test stimulus applied to a localised point at the epicardial portion of the strand a time delay, Δt, after the conditioning stimulus for the control condition. In Figure 3A, the test stimulus was applied sufficiently early (Δt = 75 ms) after the previous excitation that the tissue surrounding the stimulus site did not have time to recover enough for re-excitation to occur. As a consequence, a bi-directional conduction block was observed. In Figure 3B, the test stimulus was applied within the vulnerable window (Δt = 80 ms) that produced a unidirectional block. It is nevertheless notable that the unidirectional block occurred in the retrograde direction rather than in the anterograde direction of the conditioning wave, as observed in a homogeneous 1D strand (Zhang and Holden, 1997). This is presumably because at the test stimulus site, towards the

retrograde direction, lie endocardial cells which have a longer APD and thus need longer time to recover. However, towards the anterograde direction are epicardial cells, which have a shorter APD and thus recover excitability more rapidly. Accordingly, the excitation wave evoked by the test stimulation could only propagate towards the anterograde direction. In two-dimensions, irrespective of direction, unidirectional conduction block is an essential factor to generate re-entrant excitation. In Figure 3C, the test stimulus was applied well after the tissue surrounding the stimulus site (in both anterograde and retrograde directions) had enough time to recover from the previous excitation (Δt = 82 ms) and, consequently, bi-directional conduction was observed, though there is a considerable conduction delay in the retrograde direction as the endocardial section has longer APD and thus longer refractory period and less excitability. Figure 3D shows the width of the vulnerable time window, during which a test stimulus applied at the epicardial portion of the tissue strand resulted in unidirectional conduction block under control and different anaesthetic conditions. The computed vulnerable window was increased by the actions of anaesthetics, by more than 5%, 10% and 26% for halothane, isoflurane and sevoflurane, respectively (Figure 3D). The increased vulnerable window was due to an augmented transmural gradient of ERP as shown in Figure 2.

Spatial vulnerability of tissue to sustain re-entry

A premature test stimulus (S2) during the vulnerable window in 2D tissue produced unidirectional conduction leading to the genesis of paired re-entrant excitation waves (spiral waves) rotating in opposite directions as shown in Figure 5. However, the evoked re-entrant pairs require a certain size of substrate of the tissue to be sustained. The critical size of the substrate can be measured as the minimal spatial length of S2 required to sustain the evoked re-entry pathway (see Methods). Using the 2D model we then quantified the minimal length

of a S2 stimulus that provides sufficient substrates to accommodate a re-entrant circuit for control and anaesthetic conditions. Such a minimal length measures reciprocally the spatial vulnerability of ventricular tissue to re-entry. The results are shown in Figure 4, which presents snapshots of the formation of re-entrant wavelets corresponding to the S2 stimulus with varied sizes under control condition. In Figure 4A, the length of the S2 stimulus was 4 mm. The S2-evoked excitation wave propagated unidirectionally towards the retrograde direction of the conditioning wave with each of its two ends forming tips of a pair of spiral waves (Figure 4A). However, as the size of S2 was small, there was not sufficient tissue to accommodate the paths of the two tips. Consequently the two tips collided when they met resulting in self-termination of the two spiral waves. In Figure 4B, the length of the S2 stimulus was 5 mm, just above the critical size (4.6 mm). In this case, there was sufficient tissue to accommodate the paths of the two tips, and the two spiral waves were sustained.

The estimated minimal spatial length of S2 required to facilitate and maintain re-entry in control and anaesthetic conditions is shown in Figure 4C. In all anaesthetic cases, shortening of APD and ERP decreases the wavelength (the product of APD and conduction velocity) of the ventricular excitation wave, and thus reduced markedly the minimal length of S2 with halothane having the greatest effect, demonstrating an increased susceptibility to arrhythmia. This supports the notion that in tissue exposed to anaesthetics, re-entrant excitation can occur and be maintained more easily than in control tissue.

Dynamics of a spiral wave

The dynamics of re-entrant spiral waves in the 2D tissue model are also modulated by the actions of the anaesthetics. In 2D tissue simulations, due to heterogeneous electrical properties of the tissue, the S2-evoked spiral waves are non-stationary, with their tips (the functional singularity of the tissue acting as the origin of re-entrant excitation waves)

meandering in a large area. Due to the limited spatial size of the tissue, the spiral waves self-terminate when their tips drift out of the tissue's boundary. In both the control and anaesthetic conditions, the simulated spiral waves meander, leading to self-termination with a finite lifespan. As the anaesthetics reduce the tissue's spatial heterogeneity, the tip of spiral waves meander more slowly compared to the control condition, which results in a prolonged lifespan. Figure 5 shows the space-time plot of tip trajectory of spiral waves for control and anaesthetic conditions (time goes vertically in the z direction, space goes horizontally in the x-y plane). In simulations, halothane, unlike the other two anaesthetics, altered the tissue's transmural heterogeneity and stabilized re-entrant spiral waves by reducing the drafting velocity of their tips. As a consequence, the lifespan of the re-entrant spiral wave was prolonged by about 25%. With all three anaesthetics, the rate of re-entrant excitation waves was accelerated. The measured re-entrant excitation wave cycle was 140 ms under control conditions, which increased to 110 ms in the halothane condition.

Discussion

The cardiovascular complications of volatile anaesthetics such as contractile depression and an increased susceptibility to arrhythmia have been known for many years (see Introduction) however, the mechanisms underlying the pro-arrhythmic effects of volatile anaesthetics are still unknown. The aim of these studies was to determine whether regional differences in anaesthetic-induced changes in I_{Ca}, I_{to} and I_{ss} could potentially contribute to a pro-arrhythmic state in ventricular tissue.

In the present study, we performed a series of biophysical simulations based on our previous experimental data (Rithalia et al., 2004) to evaluate the functional impact of halothane, isoflurane and sevoflurane on APD, transmural dispersion of ventricular ADP and ERP, ventricular conduction and vulnerability of tissue to unidirectional conduction block and maintenance of re-entrant excitation. The dynamic behaviour of re-entry was also characterised. Our major findings are that: (i) the anaesthetic-induced changes in rat ventricular action potential profiles and APD could be sufficiently accounted for by the changes in I_{to}, I_{ss} and I_{Ca}- the simulated APD reduction for both endocardial and epicardial cells was quantitatively close to experimental data; (ii) the simulated reduction in APD is non-uniform with a greater decrease in endocardial than in epicardial cells leading to reduced transmural APD dispersion. However, the transmural ERP dispersion was altered differently; with the exception of halothane, isoflurane and sevoflurane augmented the transmural ERP dispersion; (iii) the three anaesthetics increased the tissue's vulnerability to genesis of unidirectional conduction block in response to a premature stimulus. Such an increased vulnerability was due to increased dispersion of ventricular effective repolarisation as shown in Figure 2; (iv) all anaesthetics decreased the critical mass of ventricular substrate necessary to facilitate and sustain re-entry due to abbreviated APD and ERP; and (v) they accelerated re-entrant excitation. Halothane also prolonged the life span of re-entry. These findings

substantiate a causative link between the actions of the three anaesthetics on ion channel conductance and cellular electrical action potentials, and offer a potential explanation for increased susceptibility of ventricular tissue to re-entry and perpetuation of re-entrant arrhythmia under the conditions of anaesthesia.

Mechanisms of pro-arrhythmogenesis

Halothane and other anaesthetics have anti- and pro-arrhythmic effects at supra-ventricular and ventricular levels although arrhythmias induced or facilitated by halothane are thought to be due to a re-entrant excitation wave (Atlee and Bosnjak, 1990). The present study suggests that the pro-arrhythmic effects of halothane and the other two anaesthetics arise as a consequence of changes in several functional aspects. First, the impact of halothane on surface membrane ion channel currents increased the susceptibility of the tissue to initiation and formation of re-entry. Tissue susceptibility can be indexed by its temporal and spatial vulnerability. While temporal vulnerability is mainly determined by the repolarisation phase of action potentials and other factors, spatial vulnerability is mainly determined by the wavelength of the excitation wave (Rensma et al., 1988; Zhang et al., 2008). In our simulations, all three anaesthetics increased the tissue's temporal vulnerability to unidirectional conduction block. Such an increased temporal vulnerability occurred via an augmented dispersion in ventricular effective repolarisation. Halothane, like isoflurane and sevoflurane, abbreviated ventricular repolarisation. This contributed to a decreased wavelength of ventricular excitation wave, resulting in a decrease in the critical size of re-entrant substrates and thus increased the tissue's spatial vulnerability to re-entry. Pro-fibrillatory effects of APD reduction have been seen in the effects of vagal stimulation or acetylcholine on initiation of re-entrant excitation waves in cardiac tissues (Nattel, 2002). Secondly, actions of halothane modulated the dynamics of re-entrant spiral wave by reducing

the drifting velocity of the tip of spiral wave. Consequently, a re-entrant spiral wave becomes more stationary and will therefore have a prolonged lifespan. Thirdly, actions of halothane increased the frequency of re-entrant excitation, which may lead to more rapid but weaker ventricular mechanical contractions.

Potential limitations of these simulations

The limitations of the mathematical model used in these studies have been discussed in depth previously (Pandit et al., 2001) and so shall not be reiterated here. However, in our multicellular tissue model, although we have considered transmural heterogeneity in rat ventricular electrical properties, we have assumed isotropic cell-to-cell electrical coupling. Possible anisotropic intercellular electrical coupling in rat ventricle was not investigated. In addition, volatile anaesthetics alter cell-to-cell conduction through gap-junction coupling, with more depression of transverse than longitudinal conduction which would tend to increase the anisotropic ratio (Brugada et al., 1991). These effects may play an important role in the initiation and perpetuation of re-entry.

It should also be noted that these data simulate the effects of anaesthetics on rat ventricular tissue which has a relatively short triangular action potential whereas that of human ventricular tissue has a longer action potential characterised by a more pronounced plateau. This is a consequence of differences in the level of expression or absence/presence of certain ion channels (e.g. the rapid and slow components of the delayed K^+ channel currents I_{Kr} and I_{Ks}) in the two tissues. Repolarisation in human ventricle is driven predominately by current flow via I_{Kr} and I_{Ks} (both of which are anaesthetic sensitive; Li and Correa, 2002; Chen et al., 2002; Yamada et al., 2006) whereas in rat ventricle, I_{to}, I_{ss} and I_{K1} dominate repolarisation. Therefore as there are species differences in the expression of

anaesthetic-sensitive channels in ventricular muscle, caution should be used in extrapolating these findings in rat ventricle to human tissue.

In either the 1D or the 2D model, we did not consider possible effects of muscle mechanical contractions on ventricular electrical excitation and assumed the tissues to be stationary. However, during the time course of electrical repolarisation the ventricle contracts, which would deform tissue geometry, changes in which, together with mechano-electric feedback, may significantly alter the excitation wave propagation in ventricular tissue. A detailed computer model of rat ventricle incorporating electrophysiology, mechanical contractions and mechano-electric feedback has become available recently (Terkildsen et al., 2008), which may be a better platform for further studies into the impact of volatile anaesthetics on electrical and contratile function of ventricular muscle. However, we feel that these limitations do not alter fundamentally our conclusions regarding the possible mechanisms by which halothane, for example, may induce a pro-arrhythmic state however, further studies including anisotropic intercellular coupling and the impact of mechano-electric feedback are warranted when experimental data become available.

Conclusion

In recent years, there has been increasing awareness of the molecular basis underlying the pro-arrhythmic effects of volatile anaesthetics. Particular emphasis has been placed on anaesthetic-induced alterations of ionic channel currents and intercellular electrical coupling. In this study, based on experimentally derived data, we illustrate *in silico*, that modest changes in ion channel conductance reduce the transmural dispersion of ventricular repolarisation, enhance the propensity for arrhythmia generation and provide a substrate for re-entry circuits with a longer half life than in control conditions.

Acknowledgements

This work was supported by The British Heart Foundation, BBSRC and The Wellcome Trust, London UK. Tao Tao is supported by an Overseas Research Studentship (ORS).

References

Antzelevitch, C., Sicouri, S., Litovsky, S.H., Lukas, A., Krishnan, S.C., Di Diego, J.M., Gintant, G.A., Liu, D.W., 1991. Heterogeneity within the ventricular wall: electrophysiology and pharmacology of epicardial, endocardial and M cells. Circ. Res. 69, 1427-1449.

Atlee, J.L., Bosnjak, Z.J., 1990. Mechanisms for cardiac dysrhythmias during anesthesia. Anesthesiology 72, 347-374.

Blayney, M.R., Malins, A.F., Cooper, G.M., 1999. Cardiac arrhythmias in children during outpatient general anaesthesia for dentistry: a prospective randomised trial. Lancet 354, 1864-1866.

Bosnjak Z.J., Supan F.D., Rusch N.J., 1991. The effects of halothane, enflurane, and isoflurane on calcium current in isolated canine ventricular cells. Anesthesiology 74, 340-345.

Brugada, J., Mont, L., Boersma, L., Kirchhof, C., Allessie, M.A., 1991. Differential effects of heptanol, potassium, and tetrodotoxin on reentrant ventricular tachycardia around a fixed obstacle in anisotropic myocardium. Circulation 84, 1307-1318.

Burt, J.M., Spray, D.C., 1989. Volatile anesthetics block intercellular communication between neonatal rat myocardial cells. Circ. Res. 65, 829-837.

Chen, X., Kamakage, M., Yamada, Y., Tohse, H., Namiki, A. 2002. Inhibitory effects of volatile anaesthetics on currents produced on heterologous expression of KvLQT1 and minK in Xenopus oocytes. Vascul. Pharmacol. 39, 33-38.

Clark, R.B., Bouchard, R.A., Salinas-Stefanon, E., Sanchez-Chapula, J., Giles, W.R., 1993. Heterogeneity of action potential waveforms and potassium currents in rat ventricle. Cardiovasc. Res. 27, 1795-1799.

Davies, L.A., Gibson, C.N., Boyett, M.R., Hopkins, P.M., Harrison, S.M., 2000a. Effects of isoflurane, sevoflurane, and halothane on myofilament Ca^{2+} sensitivity and sarcoplasmic reticulum Ca^{2+} release in rat ventricular myocytes. Anesthesiology 93, 1034-1044.

Davies, L.A., Hopkins, P.M., Boyett, M.R., Harrison, S.M., 2000b. Effects of halothane on the transient outward K^{+} current in rat ventricular myocytes. Br. J. Pharmacol. 131, 223-230.

Eskinder H., Rusch N.J., Supan F.D., Kampine J.P., Bosnjak Z.J., 1991. The effects of volatile anesthetics on L- and T-type calcium channel currents in canine Purkinje cells. Anesthesiology 74, 919-926.

Fedida, D., Giles, W.R., 1991. Regional variations in action potentials and transient outward current in myocytes isolated from rabbit left ventricle. J. Physiol. 442, 191-209.

Gima, K., Rudy, Y., 2002. Ionic current basis of electrocardiographic waveforms: a model study. Circ. Res. 90, 889-896.

Harrison, S.M., Robinson, M., Davies, L.A., Hopkins, P.M., Boyett, M.R., 1999. Mechanisms underlying the inotropic action of halothane on intact rat ventricular myocytes. Br. J. Anaesth. 82, 609-621.

Hatakeyama N., Momose Y., Ito Y., 1995. Effects of sevoflurane on the contractile responses and electrophysiologic properties in canine single cardiac myocytes. Anesthesiology 82, 559-565.

Hayes E.S., Barrett T.D., Burrill D.E., Walker M.J.A., 1996. Effects of halothane and isoflurane on rat ventricular action potentials recorded *in situ*. Life Sci. 58, 1375-1385.

Huneke, R., Jungling, E., Skasa, M., Rossaint, R., Luckhoff, A., 2001. Effects of the anesthetic gases xenon, halothane, and isoflurane on calcium and potassium currents in human atrial cardiomyocytes. Anesthesiology 95, 999-1006.

Ikemoto, Y., Yatani, A., Arimura, H., Yoshitake, J., 1985. Reduction of the slow inward current of isolated rat ventricular cells by thiamylal and halothane. Acta Anaesthesiol. Scand. 29, 583-586.

Li, J., and Correa, A.M., 2002. Kinetic modulation of HERG potassium channels by the volatile anaesthetic halothane. Anesthesiology 97, 921-930.

Meiry, G., Reisner, Y., Feld, Y., Goldberg, S., Rosen, M., Ziv, N., Binah, O., 2001. Evolution of action potential propagation and repolarization in cultured neonatal rat ventricular myocytes. J Cardiovasc. Electrophysiol. 12, 1269-1277.

Nabauer M., Beuckelmann D.J, Uberfuhr P, Steinbeck G., 1996. Regional differences in current density and rate-dependent properties of the transient outward current in subepicardial and subendocardial myocytes of human left ventricle. Circulation 93, 168-177.

Nattel, S. 2002. New ideas about atrial fibrillation 50 years on. Nature 415, 219-226.

Pancrazio J.J. 1996. Halothane and isoflurane preferentially depress a slow inactivating component of Ca^{2+} channel current in guinea-pig myocytes. J. Physiol. 494, 94-103.

Pandit, S.V., Clark, R.B., Giles, W.R., Demir, S.S., 2001. A mathematical model of action potential heterogeneity in adult rat left ventricular myocytes. Biophys. J. 81, 3029-3051.

Rensma, P.L., Allessie, M.A., Lammers, W.J., Bonke, F.I., Schalij, M.J., 1988. Length of excitation wave and susceptibility to reentrant atrial arrhythmias in normal conscious dogs. Circ. Res. 62, 395-410.

Rithalia, A., Gibson, C.N., Hopkins, P.M., Harrison, S.M., 2001. Halothane inhibits contraction and action potential duration to a greater extent in subendocardial than subepicardial myocytes from the rat left ventricle. Anesthesiology 95, 1213-1219.

Rithalia, A., Hopkins, P.M., Harrison, S.M., 2004. The effects of halothane, isoflurane, and sevoflurane on Ca^{2+} current and transient outward K^{+} current in subendocardial and subepicardial myocytes from the rat left ventricle. Anesth. Analg. 99, 1615-22, table.

Salle, L., Kharche, S., Zhang, H., Brette, F., 2008. Mechanisms underlying adaptation of action potential duration by pacing rate in rat myocytes. Prog. Biophys. Mol. Biol. 96, 305-320.

Shaw, R.M., Rudy, Y., 1995. The vulnerable window for unidirectional block in cardiac tissue: characterization and dependence on membrane excitability and intercellular coupling. J Cardiovasc. Electrophysiol. 6, 115-131.

Starmer, C.F., Biktashev, V.N., Romashko, D.N., Stepanov, M.R., Makarova, O.N., Krinsky, V.I., 1993. Vulnerability in an excitable medium: analytical and numerical studies of initiating unidirectional propagation. Biophys. J. 65, 1775-1787.

Terkildsen, J.R., Niederer, S., Crampin, E.J., Smith, N.P., 2008. Using Physiome standards to couple cellular functions for rat cardiac excitation-contraction. Exp. Physiol. 93, 919-929.

Terrar, D.A., Victory, J.G.G., 1988. Effects of halothane on membrane currents associated with contraction in single myocytes isolated from guinea-pig ventricle. Br. J. Pharmacol. 94, 500-508.

Volk, T., Nguyen, T.H., Schultz, J.H., Ehmke, H., 1999. Relationship between transient outward K^+ current and Ca^{2+} influx in rat cardiac myocytes of endo- and epicardial origin. J. Physiol. 519, 841-850.

Wettwer, E., Amos, G., Gath, J., Zerkowski, H.R., Reidemeister, J.C., Ravens, U., 1993. Transient outward current in human and rat ventricular myocytes. Cardiovasc. Res 27, 1662-1669.

Workman, A.J., Kane, K.A., Rankin, A.C., 2001. The contribution of ionic currents to changes in refractoriness of human atrial myocytes associated with chronic atrial fibrillation. Cardiovasc. Res 52, 226-235.

Yamada, M., Hatakeyama, N., Malykhina, A.P., Yamazaki, M., Momose, Y., Akbarali, H.I., 2006. The effects of sevoflurane and propofol on QT intereval and heterologously expressed human ether-a-go-go related gene currents in Xenopus oocytes. Anesth. Analg. 102, 98-103.

Zhang, H., Hancox, J.C., 2004. In silico study of action potential and QT interval shortening due to loss of inactivation of the cardiac rapid delayed rectifier potassium current. Biochem. Biophys. Res Commun. 322, 693-699.

Zhang, H., Holden, A.V., 1997. One-dimensional modelling of the vulnerability to re-entry of homogeneous atrial tissue. J. Theor. Biol. 184, 117-122.

Zhang, H., Kharche, S., Holden, A.V., Hancox, J.C., 2008. Repolarisation and vulnerability to re-entry in the human heart with short QT syndrome arising from KCNQ1 mutation--a simulation study. Prog. Biophys. Mol. Biol. 96, 112-131.

Zhang, H., Winslow, R.W., Holden, A.V., 1998. Re-entrant excitation initiated in models of inhomogeneous atrial tissue. J. Theor. Biol. 191, 279-287.

	Sub-epicardium			**Sub-endocardium**	
	I_{Ca}	I_{to}	I_{SS}	I_{Ca}	I_{SS}
Halothane	-40%	-8%	+7%	-40%	+6%
Isoflurane	-20%	-8%	+4%	-20%	0
Sevoflurane	-12%	0	+8%	-12%	+8%

Table 1. Effects of halothane, isoflurane and sevoflurane on I_{Ca}, I_{to} and I_{ss} in sub-epicardial and sub-endocardial myocytes, expressed as a percentage of control.(Rithalia *et al.*, 2004)

Figure legends

Figure 1. Representative action potential recordings from sub-endocardial (solid lines) and sub-epicardial (dashed lines) left ventricular myocytes under control conditions (A) and at steady-state in the presence of 0.6 mM halothane (B). Simulated sub-endocardial and sub-epicardial action potential waveforms under control conditions (C) and following the alteration of the membrane conductance of I_{Ca}, I_{to} and I_{ss} to model the effects of halothane (D). E, mean experimental data, from ref(Rithalia *et al.*, 2004) for action potential duration at 90% repolarisation (APD_{90}) for sub-endocardial (N) and sub-epicardial (P) cells for control and halothane conditions, compared with APD_{90} values measured from simulated action potentials. F, the transmural gradient of APD from experimental data (E, from Rithalia *et al.*, 2004) or from simulated action potentials (S) under control conditions, or with halothane (Hal), isoflurane (Iso) or sevoflurane (Sevo) at steady state, expressed as a % of control. G, the effect of changes in ion conductances alone or in combination on computed APD_{90} in sub-endocardial and sub-epicardial cells. The resulting transmural gradient of APD_{90} for each of these conditions is shown in panel H.

Figure 2. (A): Computed effective refractory period (ERP) for endocardial (N) and epicardial (P) cells for control, halothane (Hal), isoflurane (Iso) and sevoflurane (Sevo) conditions. (B): Computed transmural gradient of ERP expressed as a % of control.

Figure 3. Effects of anaesthetics on the vulnerability of tissue to the genesis of unidirectional conduction block in response to a premature stimulus applied to the refractory tail of a conditioning wave. A-C: Time-space plot of an action potential propagating on a 1D transmural ventricular strand (space runs vertically from endocardium (N) to epicardium (P);

time runs horizontally). A conditioning wave was evoked by a supra-threshold stimulus applied to the endocardial end, which propagated from the endocardial to the epicardial end. After a time delay, a premature stimulus was applied. Depending on the timing, the premature stimulus evoked excitation wave either failed to propagate if it was too early (A), conduct bi-directionally if it was too late (C), or propagate unidirectionally (B) if it fell within a critical time window. D, the computed vulnerable window under control and anaesthetic conditions. All anaesthetics increase the vulnerability of the tissue to re-entry.

Figure 4. Measurement of the critical size of re-entrant pathway to initiate a re-entry circuit. A premature stimulus during the vulnerable window evokes unidirectional conduction block, which leads to the formation of a pair of counter rotating spiral wave. The spiral waves either collide leading to self-termination if the length (spatial) of the premature stimulus is not large enough to accommodate the pathway of the two tips of the spiral wave (Ai-Aiii), or survive (Bi-Biii). The minimal length of a premature stimulus, above which two spiral waves survive gives a measurement of the critical size of re-entrant substrate of the tissue. This minimal length is dependent on the wavelength of excitation (the product of APD and conduction velocity), and quantifies reciprocally the spatial vulnerability of tissue to re-entry. The smaller the critical size, the more vulnerable the tissue to reentry. C, measured critical size of re-entrant substrate under control and anaesthetic conditions. Only halothane reduced the critical size significantly, which implies that the tissue's spatial vulnerability is increased significantly by halothane.

Figure 5. Time-space plot (time runs vertically from bottom to top; space: x-y plane) of tip trajectory of re-entrant excitation waves for control (A), halothane (B), isoflurane (C) and sevoflurane (D). The tip starts from the middle of the tissue (marked by the lower thin arrow)

and terminates at the boundary of the tissue (marked by the upper thick arrow). The dashed arrow marks the drafting direction. In all cases, the re-entrant excitation wave is non-stationary with its tip meandering within the tissue. When its tip hits the tissue's boundary, the re-entrant excitation wave self-terminates. Halothane, unlike the other two anaesthetics, slowed down the tip's drifting velocity prolonging the lifespan of the re-entrant wave.

Appendix

Cell Geometry

C_m	Membrane capacitance
V_{cell}	Cell volume
V_i	Myoplasmic volume
V_{rel}	Volume of junctional SR
V_{sub}	Subspace volume
V_{up}	Volume of network SR

Ionic Concentrations

$[Ca^{2+}]_i$	Myoplasmic Ca^{2+} concentration
$[Ca^{2+}]_o$	Extracellular Ca^{2+} concentration
$[Ca^{2+}]_{rel}$	Ca^{2+} concentration in the junctional SR
$[Ca^{2+}]_{sub}$	Subspace Ca^{2+} concentration
$[Ca^{2+}]_{up}$	Ca^{2+} concentration in the network SR
$[K^+]_i$	Myoplasmic K^+ concentration
$[K^+]_o$	Extracellular K^+ concentration
$[Na^+]_i$	Myoplasmic Na^+ concentration
$[Na^+]_o$	Extracellular Na^+ concentration

Equilibrium (Reversal) Potentials

E_{CaL}	Apparent reversal potential of I_{CaL}
E_{Na}	Apparent reversal potential of I_{Na}
E_K	Apparent reversal potential of I_K

Sarcolemmal Ionic Currents

Ca_{inact}	Ca^{2+}-inactivation gating variable
d	Activation gating variable for I_{CaL}
d_{NaCa}	Denominator constant for I_{NaCa}
$f_{11\infty}$	Fast inactivation gating variable for I_{CaL}

f_{12}	Slow inactivation gating variable for I_{CaL}
g_{BCa}	Maximum I_{BCa} conductance
g_{BK}	Maximum I_{BK} conductance
g_{BNa}	Maximum I_{BNa} conductance
g_{CaL}	Maximum I_{CaL} conductance
g_f	Maximum I_f conductance
g_{K1}	Maximum I_{K1} conductance
g_{Na}	Maximum I_{Na} conductance
g_{ss}	Maximum I_{ss} conductance
g_{to}	Maximum I_{to} conductance
h	Fast inactivation gating variable for I_{Na}
I_{CaP_bar}	Maximum I_{CaP} current
I_{NaK_bar}	Maximum I_{NaK} current
j	Slow inactivation gating variable for I_{Na}
$K_{m,K}$	Half-maximum K^+ binding constant for I_{NaK}
$K_{m,Na}$	Half-maximum Na^+ binding constant for I_{NaK}
k_{NaCa}	Scaling factor for I_{NaCa}
m	Activation gating variable for I_{Na}
r	Activation gating variable for I_{to}
r_{ss}	Activation gating variable for I_{ss}
s	Fast inactivation gating variable for I_{to}
s_{slow}	Slow inactivation gating variable for I_{to}
s_{ss}	Inactivation gating variable for I_{ss}
y	Inactivation gating variable for I_f
y_{NaCa}	Position of energy barrier controlling voltage dependence of I_{NaCa}

Ca^{2+} Diffusion

J_{xfer}	Ca^{2+} diffusion flux from subspace to myoplasm
τ_{xfer}	Time constant for Ca^{2+} diffusion from subspace to myoplasm

SR Function

J_{rel}	Ca^{2+} release flux from the junctional SR to subspace
J_{tr}	Ca^{2+} transfer flux from the network SR to junctional SR

J_{up}	Ca^{2+} uptake flux from the myoplasm to network SR
K_a^+	RyR P_{c1}-P_{o1} rate constant
K_a^-	RyR P_{o1}-P_{c1} rate constant
K_b^+	RyR P_{o1}-P_{o2} rate constant
K_b^-	RyR P_{o2}-P_{o1} rate constant
K_c^+	RyR P_{o1}-P_{c2} rate constant
K_c^-	RyR P_{c2}-P_{o1} rate constant
K_{fb}	Forward half-saturation constant for Ca^{2+}-ATPase
K_{rb}	Backward half-saturation constant for Ca^{2+}-ATPase
K_{SR}	Scaling factor for Ca^{2+}-ATPase
m_{SR}	RyR Ca^{2+} cooperativity parameter P_{o1}-P_{o2}
n_{SR}	RyR Ca^{2+} cooperativity parameter P_{c1}-P_{o1}
N_{fb}	Forward cooperativity constant for Ca^{2+}-ATPase
N_{rb}	Reverse cooperativity constant for Ca^{2+}-ATPase
P_{c1}	Fraction of channels in state P_{c1}
P_{c2}	Fraction of channels in state P_{c2}
P_{o1}	Fraction of channels in state P_{o1}
P_{o2}	Fraction of channels in state P_{o2}
τ_{tr}	Time constant for Ca^{2+} transfer from the network SR to junctional SR
v_1	Maximum RyR channel Ca^{2+} flux
v_{maxf}	Ca^{2+}-ATPase forward rate parameter
v_{maxr}	Ca^{2+}-ATPase reverse rate parameter

Ca^{2+} Buffering

$[CMDN]_{tot}$	Total calmodulin concentration
$[CSQN]_{tot}$	Total calsequestrin concentration
$[EGTA]_{tot}$	Total myoplasm EGTA concentration
$[HTRPN]_{tot}$	Total troponin high-affinity site concentration
htrpn	Concentration of Ca^{2+}-bound high-affinity troponin sites
K_m^{CMDN}	Ca^{2+} half-saturation constant for calmodulin
K_m^{CSQN}	Ca^{2+} half-saturation constant for calsequestrin
K_m^{EGTA}	Ca^{2+} half-saturation constant for EGTA
K^+_{htrpn}	Ca^{2+} on rate for troponin high-affinity sites
K^-_{htrpn}	Ca^{2+} off rate for troponin high-affinity sites

K^+_{ltrpn}	Ca^{2+} on rate for troponin low-affinity sites
K^-_{ltrpn}	Ca^{2+} off rate for troponin low-affinity sites
$[LTRPN]_{tot}$	Total troponin low-affinity site concentration
ltrpn	Concentration of Ca^{2+}-bound low-affinity troponin sites

Model constants

Model parameters	**Values**
$[Ca^{2+}]_o$ (mM)	1.2
C_m (μF)	100e-6
$[CMDN]_{tot}$ (mM)	50.0e-3
$[CSQN]_{tot}$ (mM)	15
d_{NaCa} $(mM)^{-4}$	0.0001
$[EGTA]_{tot}$ (mM)	10
F $(C \cdot mol^{-1})$	96,487
g_{BCa} (μS)	3.24e-5
g_{BK} (μS)	13.8e-5
g_{BNa} (μS)	8.015e-5
g_{CaL} (μS)	0.031
g_f (μS)	0.00145
g_{K1} (μS)	0.024
g_{Na} (μS)	0.8
g_{ss} (μS)	0.007
g_{to} (μS)	0.035
$[HTRPN]_{tot}$ (mM)	140e-3
I_{CaP_bar} (nA)	0.004
$I_{NaK\text{-}bar}$ (nA)	0.08
K_a^+ $(mM^{-4}s^{-1})$	12.15e12
K_a^- (s^{-1})	0.576e3
K_b^+ $(mM^{-3}s^{-1})$	4.05e9
K_b^- (s^{-1})	1.93e3
K_c^+ (s^{-1})	0.1e3

K_c^- (s^{-1})	0.0008e3
K_{fb} (mM)	0.168e-3
K^+_{htrpn} ($mM^{-1}s^{-1}$)	200e3
K^-_{htrpn} (s^{-1})	66e-3
K^+_{ltrpn} ($mM^{-1}s^{-1}$)	40e3
K^-_{ltrpn} (s^{-1})	0.04e3
K_m^{CMDN} (mM)	2.38e-3
K_m^{CSQN} (mM)	0.8
K_m^{EGTA} (mM)	1.5e-4
$K_{m,K}$ (mM)	1.5
$K_{m,Na}$ (mM)	10
k_{NaCa} (mM^{-4})	0.9984e-5
$[K^+]_o$ (mM)	5.4
K_{rb} (mM)	3.29
K_{SR}	1.0
$[LTRPN]_{tot}$ (mM)	70e-3
m_{SR}	3
$[Na^+]_0$ (mM)	140
N_{fb}	1.2
N_{rb}	1.0
n_{SR}	4
R (mJ/mol K)	8314
T (K)	295
τ_{tr} (s)	0.5747e-3
τ_{xfer} (s)	26.7e-3
v_1 (s^{-1})	1.8e3
V_{cell} (pl)	16
V_i (pl)	9.36
v_{maxf} (mM s^{-1})	0.4e-1
v_{maxr} (mM s^{-1})	0.9
V_{rel} (pl)	0.056
V_{sub} (pl)	0.0012
V_{up} (pl)	0.504
Y_{NaCa}	0.5

Equations

Sarcolemmal Ionic Current

Na^+ current

$$I_{Na} = g_{Na} m^3 hj(V - E_{Na}) \quad (1)$$

$$\bar{m} = \frac{1}{1 + e^{(V+45.0)/-6.5}} \quad (2)$$

$$\bar{h} = \bar{j} = \frac{1}{1 + e^{(V+76.1)/6.07}} \quad (3)$$

$$E_{Na} = \frac{RT}{F} \ln \frac{[Na^+]_o}{[Na^+]_i} \quad (4)$$

$$\frac{dm}{dt} = \frac{\bar{m} - m}{\tau_m} \quad (5)$$

$$\frac{dh}{dt} = \frac{\bar{h} - h}{\tau_h} \quad (6)$$

$$\frac{dj}{dt} = \frac{\bar{j} - j}{\tau_j} \quad (7)$$

$$\tau_m = \frac{0.00136}{\frac{0.32(V + 47.13)}{1.0 - e^{-0.1(V+47.13)}} + 0.08e^{V/11}} \quad (8)$$

if V>=-40 mV

$$\tau_h = 0.0004537(1.0 + e^{(V+10.66)/11.1}) \quad (9)$$

$$\tau_j = \frac{0.01163(1.0 + e^{-0.1(V+32.0)})}{e^{-2.535\times10^{-7}V}} \quad (10)$$

else if V<=-40 mV

$$\tau_h = \frac{0.00349}{0.135e^{(V+80.0)/6.8} + 3.56e^{0.079V} + 3.1\times10^5 e^{0.35V}} \quad (11)$$

$$\tau_j = 0.00349 \div \left[\frac{V + 37.78}{1.0 + e^{0.311(V+79.23)}} (-127140e^{0.2444V} - 3.474\times10^{-5} e^{-0.04391V}) + \frac{0.1212e^{-0.01052V}}{1.0 + e^{-0.1378(V+40.14)}} \right] \quad (12)$$

L-type Ca^{2+} current

$$I_{Ca,L} = g_{Ca,L} d\left[(0.9 + \frac{Ca_{inact}}{10.0}) f_{11} + (0.1 - \frac{Ca_{inact}}{10.0}) f_{12}\right](V - E_{CaL}) \quad (13)$$

$$\bar{d} = \frac{1}{1 + e^{(V+15.3)/-5.0}} \quad (14)$$

$$\bar{f_{11}} = \bar{f_{12}} = \frac{1}{1 + e^{(V+26.7)/5.4}} \quad (15)$$

$$E_{CaL} = 65.0 \quad (16)$$

$$\tau_d = 0.00305 e^{-0.0045(V+7.0)^2} + 0.00105 e^{-0.002(V-18.0)^2} + 0.00025 \quad (17)$$

$$\tau_{f11} = 0.105 e^{-((V+45.0)/12.0)^2} + \frac{0.04}{(1.0 + e^{(-V+25.0)/25.0})} + \frac{0.015}{(1.0 + e^{(V+75.0)/25.0})} + 0.017 \quad (18)$$

$$\tau_{f12} = 0.041 e^{-((V+47.0)/12.0)^2} + \frac{0.08}{(1.0 + e^{(-V+55.0)/-5.0})} + \frac{0.015}{(1.0 + e^{(V+75.0)/25.0})} + 0.017 \quad (19)$$

$$\bar{Ca}_{inact} = \frac{1.0}{(1.0 + [Ca^{2+}]_{ss}/0.01)} \quad (20)$$

$$\tau_{Cainact} = 0.009 \quad (21)$$

$$\frac{dd}{dt} = \frac{\bar{d} - d}{\tau_d} \quad (22)$$

$$\frac{df_{11}}{dt} = \frac{\bar{f_{11}} - f_{11}}{\tau_{f11}} \quad (23)$$

$$\frac{df_{12}}{dt} = \frac{\bar{f_{12}} - f_{12}}{\tau_{f12}} \quad (24)$$

$$\frac{dCa_{inact}}{dt} = \frac{\bar{Ca}_{inact} - Ca_{inact}}{\tau_{Cainact}} \quad (25)$$

Ca^{2+}-independent transient outward K^+ current

$$I_{to} = g_{to} r(as + bs_{slow})(V - E_K) \quad (26)$$

$$\bar{r} = \frac{1}{1 + e^{(V+10.6)/-11.42}} \quad (27)$$

$$\bar{s} = \bar{s}_{slow} = \frac{1}{1 + e^{(V+45.3)/6.8841}} \quad (28)$$

$$\tau_r = \frac{1}{45.16e^{0.03577(V+50.0)} + 98.9e^{-0.1(V+38.0)}} \quad (29)$$

$$\tau_s = 0.35e^{-(V+70.0/15.0)^2} + 0.035 \quad (30)$$

$$\tau_{Sslow} = 3.7e^{-(V+70.0/30.0)^2} + 0.035 \quad (31)$$

$$\frac{dr}{dt} = \frac{\bar{r} - r}{\tau_r} \quad (32)$$

$$\frac{ds}{dt} = \frac{\bar{s} - s}{\tau_s} \quad (33)$$

$$\frac{ds_{slow}}{dt} = \frac{\bar{s}_{slow} - s_{slow}}{\tau_{Sslow}} \quad (34)$$

$$E_K = \frac{RT}{F}\ln\frac{[K+]_o}{[K+]_i} \quad (35)$$

a=0.886; b=0.114

Steady-state outward K^+ current

$$I_{ss} = g_{ss} r_{ss} s_{ss} (V - E_K) \quad (36)$$

$$\bar{r}_{ss} = \frac{1}{1 + e^{(V+11.5)/-11.82}} \quad (37)$$

$$\bar{s}_{ss} = \frac{1}{1 + e^{(V+87.5)/10.3}} \quad (38)$$

$$\tau_{rss} = \frac{10.0}{45.16e^{0.03577(V+50.0)} + 98.9e^{-0.1(V+38.0)}} \quad (39)$$

$$\tau_{Sss} = 2.1 \quad (40)$$

$$\frac{dr_{ss}}{dt} = \frac{\bar{r}_{ss} - r_{ss}}{\tau_{rss}} \quad (41)$$

$$\frac{ds_{ss}}{dt} = \frac{\bar{s}_{ss} - s_{ss}}{\tau_{Sss}} \quad (42)$$

Inwardly rectifying K^+ current

$$I_{K1} = \left[\frac{48}{(e^{(V+37)/25} + e^{(V+37)/-25} + 10}\right] \bullet \left[\frac{0.0001}{1 + e^{(V-EK-76.77)/-17}}\right] + \frac{g_{K1}(V - E_K - 1.73)}{(1 + e^{1.613F((V-E_K-1.73)/RT)}) \bullet (1 + e^{[K^+]_o - 0.9988/-0.124})} \quad (43)$$

Hyperpolarization-activated current

$$I_f = g_f y[f_{Na}(V - E_{Na}) + f_K(V - E_K)] \quad (44)$$

$$y_\infty = \frac{1}{1 + e^{(V+138.6)/10.48}} \quad (45)$$

$$f_{Na} = 0.2, f_K = 1 - f_{Na} \quad (46)$$

$$\frac{dy}{dt} = \frac{y_\infty - y}{\tau_y} \quad (47)$$

$$\tau_y = \frac{1}{(0.11885e^{(V+80.0)/28.37} + 0.56236e^{(V+80.0)/-14.19})} \quad (48)$$

Background currents

$$I_{BNa} = g_{BNa}(V - E_{Na}) \quad (49)$$

$$I_{BK} = g_{BK}(V - E_K) \quad (50)$$

$$I_{BCa} = g_{BCa}(V - E_{CaL}) \quad (51)$$

$$I_B = I_{BNa} + I_{BCa} + I_{BK} \quad (52)$$

Na^+-K^+ pump current

$$I_{NaK} = \bar{I}_{NaK}\left(\frac{1.0}{1.0 + 0.1245e^{0.1VF/RT} + 0.0365\sigma e^{VF/RT}}\right) \bullet \left(\frac{[K^+]_o}{[K^+]_o + k_{m,K}}\right) \quad (53)$$

$$\sigma = \frac{e^{[Na^+]_o/67.3} - 1.0}{7.0} \quad (54)$$

Sarcolemmal Ca^{2+} pump current

$$I_{CaP} = \bar{I}_{CaP}\left(\frac{[Ca^{2+}]_i}{[Ca^{2+}]_i + 0.0004}\right) \quad (55)$$

Na^+-Ca^{2+} exchanger current

$$I_{NaCa} = k_{NaCa} \bullet \frac{[Na^+]_i^3 \bullet [Ca^{2+}]_o \bullet e^{0.03743V\gamma_{NaCa}} - [Na^+]_o^3 \bullet [Ca^{2+}]_i \bullet e^{0.03743V(\gamma_{NaCa}-1.0)}}{1.0 + d_{NaCa} \bullet ([Na^+]_i^3 \bullet [Ca^{2+}]_o + [Na^+]_o^3 \bullet [Ca^{2+}]_i)} \quad (56)$$

Membrane potential

$$\frac{dV}{dt} = \frac{-(I_{Na} + I_{CaL} + I_{to} + I_{ss} + I_f + I_{K1} + I_B + I_{NaK} + I_{NaCa} + I_{CaP})}{C_m} \quad (57)$$

Intracellular Ca^{2+} Dynamics

Ca^{2+} release channel in sarcoplasmic reticulum

$$\frac{dP_{C1}}{dt} = -K_a^{+}[Ca^{2+}]_{sub}{}^{n} P_{C1} + K_a^{-} P_{O1} \quad (58)$$

$$\frac{dP_{O1}}{dt} = K_a^{+}[Ca^{2+}]_{sub}{}^{n} P_{C1} - K_a^{-} P_{O1} - K_b^{+}[Ca^{2+}]_{sub}{}^{m} P_{O1} + K_b^{-} P_{O2} - K_c^{+} P_{O1} + K_c^{-} P_{O2} \quad (59)$$

$$\frac{dP_{O2}}{dt} = K_b^{+}[Ca^{2+}]_{sub}{}^{m} P_{O1} - K_b^{-} P_{O2} \quad (60)$$

$$\frac{dP_{C2}}{dt} = K_c^{+} P_{O1} - K_c^{-} P_{C2} \quad (61)$$

$$J_{rel} = v_1 (P_{O1} + P_{O2})([Ca^{2+}]_{rel} - [Ca^{2+}]_{sub}) \quad (62)$$

SERCA2a Ca^{2+} pump

$$f_b = ([Ca^{2+}]_i / K_{fb})^{N_{fb}} \quad (63)$$

$$r_b = ([Ca^{2+}]_{up} / K_{rb})^{N_{rb}} \quad (64)$$

$$J_{up} = K_{SR} \frac{v_{\max,f} f_b - v_{\max,r} r_b}{1 + f_b + r_b} \quad (65)$$

Intracellular and SR Ca^{2+} fluxes

$$J_{tr} = \frac{[Ca^{2+}]_{up} - [Ca^{2+}]_{rel}}{\tau_{tr}} \quad (66)$$

$$J_{xfer} = \frac{[Ca^{2+}]_{sub} - [Ca^{2+}]_i}{\tau_{xfer}} \quad (67)$$

$$J_{trpn} = \frac{d[HTRPNCa]}{dt} + \frac{d[LTRPNCa]}{dt} \quad (68)$$

$$\frac{d[HTRPNCa]}{dt} = K^{+}_{htrpn}[Ca^{2+}]_i([HTRPN]_{tot} - [HTRPNCa]) - K^{-}_{htrpn}[HTRPNCa] \quad (69)$$

$$\frac{d[LTRPNCa]}{dt} = K^{+}_{ltrpn}[Ca^{2+}]_i([LTRPN]_{tot} - [LTRPNCa]) - K^{-}_{ltrpn}[LTRPNCa] \quad (70)$$

Intracellular ion concentrations

$$\frac{d[Na^+]_i}{dt} = -(I_{Na} + I_{BNa} + 3I_{NaCa} + 3I_{NaK} + I_{f,Na})\frac{1.0}{V_i F} \quad (71)$$

$$\frac{d[K^+]_i}{dt} = -(I_{ss} + I_{BK} + I_t + I_{K1} + I_{f,K} - 2I_{NaK})\frac{1.0}{V_i F} \quad (72)$$

$$\frac{d[Ca^{2+}]_i}{dt} = \beta_i\{J_{xfer} - J_{up} - J_{trpn} - (I_{BCa} - 2I_{NaCa} + I_{CaP})\frac{1.0}{2V_i F}\} \quad (73)$$

$$\beta_i = \left\{1 + \frac{[CMDN]_{tot} K_m^{CMDN}}{(K_m^{CMDN} + [Ca^{2+}]_i)^2} + \frac{[EGTA]_{tot} K_m^{EGTA}}{(K_m^{EGTA} + [Ca^{2+}]_i)^2}\right\}^{-1} \quad (74)$$

$$\beta_{sub} = \left\{1 + \frac{[CMDN]_{tot} K_m^{CMDN}}{(K_m^{CMDN} + [Ca^{2+}]_{sub})^2}\right\}^{-1} \quad (75)$$

$$\beta_{rel} = \left\{1 + \frac{[CSQN]_{tot} K_m^{CSQN}}{(K_m^{CSQN} + [Ca^{2+}]_{rel})^2}\right\}^{-1} \quad (76)$$

$$\frac{d[Ca^{2+}]_{sub}}{dt} = \beta_{sub}\{J_{rel}\frac{V_{rel}}{V_{sub}} - J_{xfer}\frac{V_i}{V_{sub}} - (I_{CaL})\frac{1.0}{2V_{sub}F}\} \quad (77)$$

$$\frac{d[Ca^{2+}]_{rel}}{dt} = \beta_{rel}\{J_{tr} - J_{rel}\} \quad (78)$$

$$\frac{d[Ca^{2+}]_{up}}{dt} = J_{up}\frac{V_i}{V_{up}} - J_{tr}\frac{V_{rel}}{V_{up}} \quad (79)$$

Equations for the endocardial cell

Following changes are made to the above epicardial cell model parameters and equations for the formulation of the endocardial cell.

Na^+ current

$$g_{Na,endo} = 1.33 g_{Na,epi} \quad (80)$$

Ca^{2+}-independent transient outward K^+ current

$$g_{to,endo} = 0.4647 g_{to,epi} \quad (81)$$

$$\tau_{s,endo} = 0.55 e^{-((V+70.0)/25.0)^2} + 0.049 \quad (82)$$

$$\tau_{Sslow,endo} = 3.3 e^{-((V+70.0)/30.0)^2} + 0.049 \quad (83)$$

$$a_{endo} = 0.583 \; ; \; b_{endo} = 0.417$$

Equations for 1D ventricle strand

$$\frac{\partial V_m}{\partial t} = -I_{tot} / C_m + \nabla \bullet (D \nabla V_m) \quad (84)$$

Equations for the pseudo ECG

$$\phi_e(x', y', z') = \frac{a^2 \sigma_i}{4\sigma_e} \int (-\nabla V_m) \bullet \left[\nabla \frac{1}{r} \right] dx \quad (85)$$

$$r = \sqrt{(x-x')^2 + (y-y')^2 + (z-z')^2} \quad (86)$$

$$\nabla V_m = (V_m(r+dx) - Vm(r-dx))/(2dx) \quad (87)$$

$$\nabla(1/r) = (1/(r+dx) - 1/(r-dx))/(2dx) \quad (88)$$

Fig 1

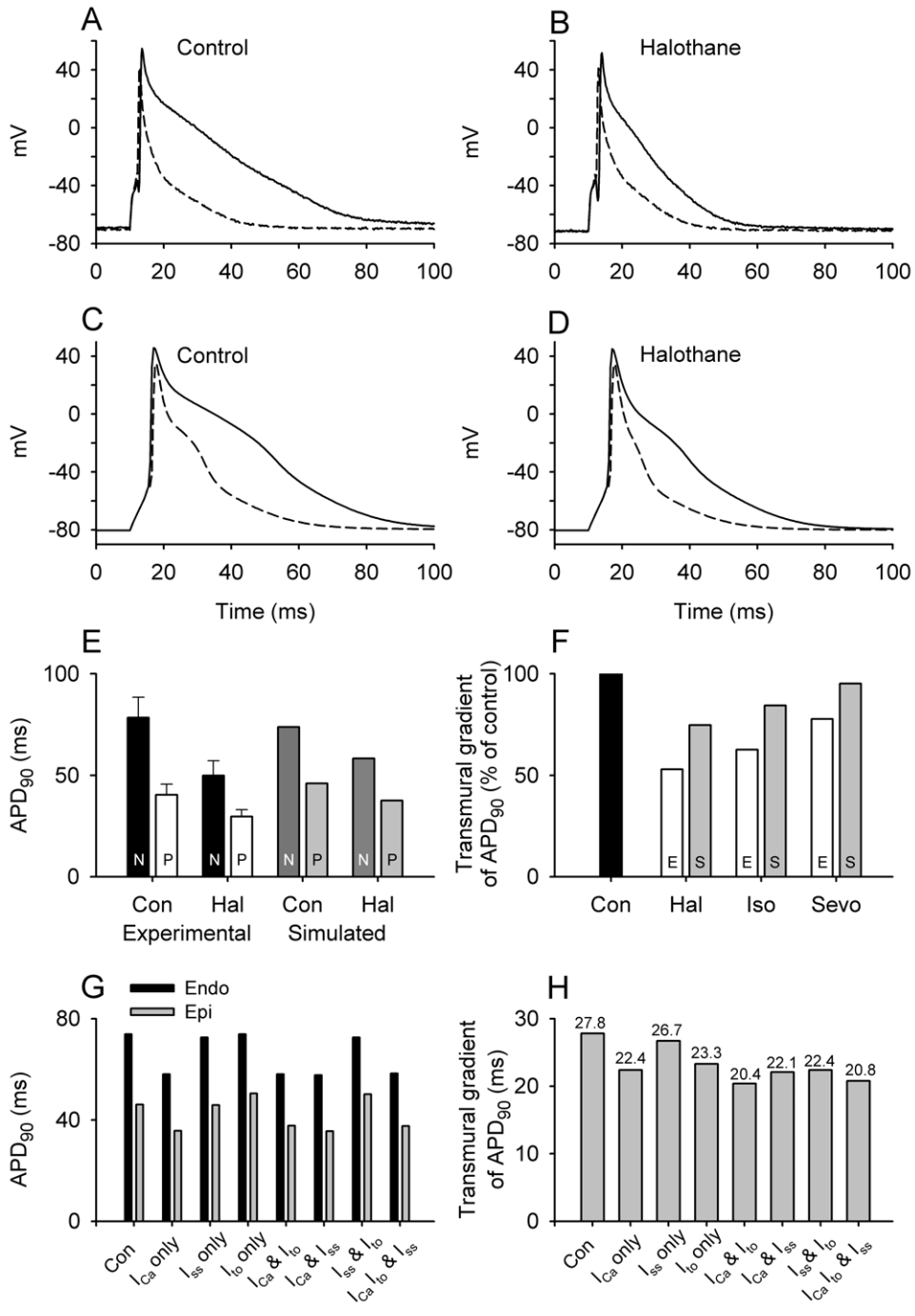

Fig 2

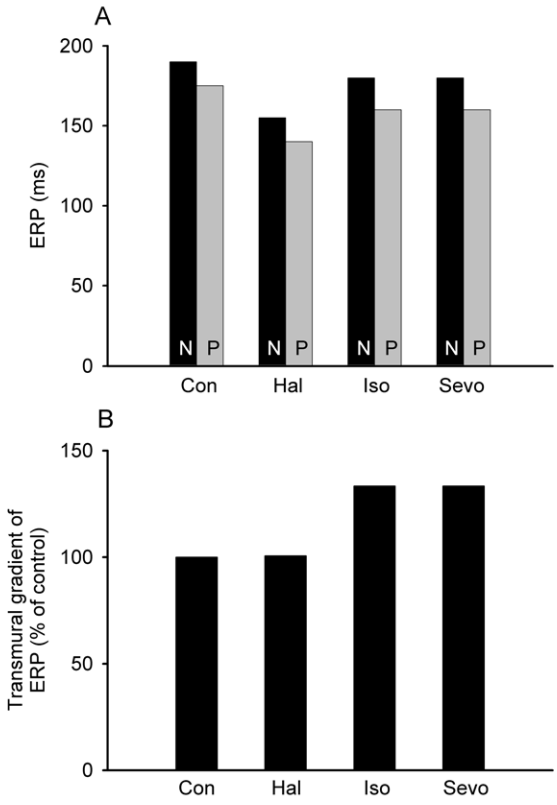

Fig 3

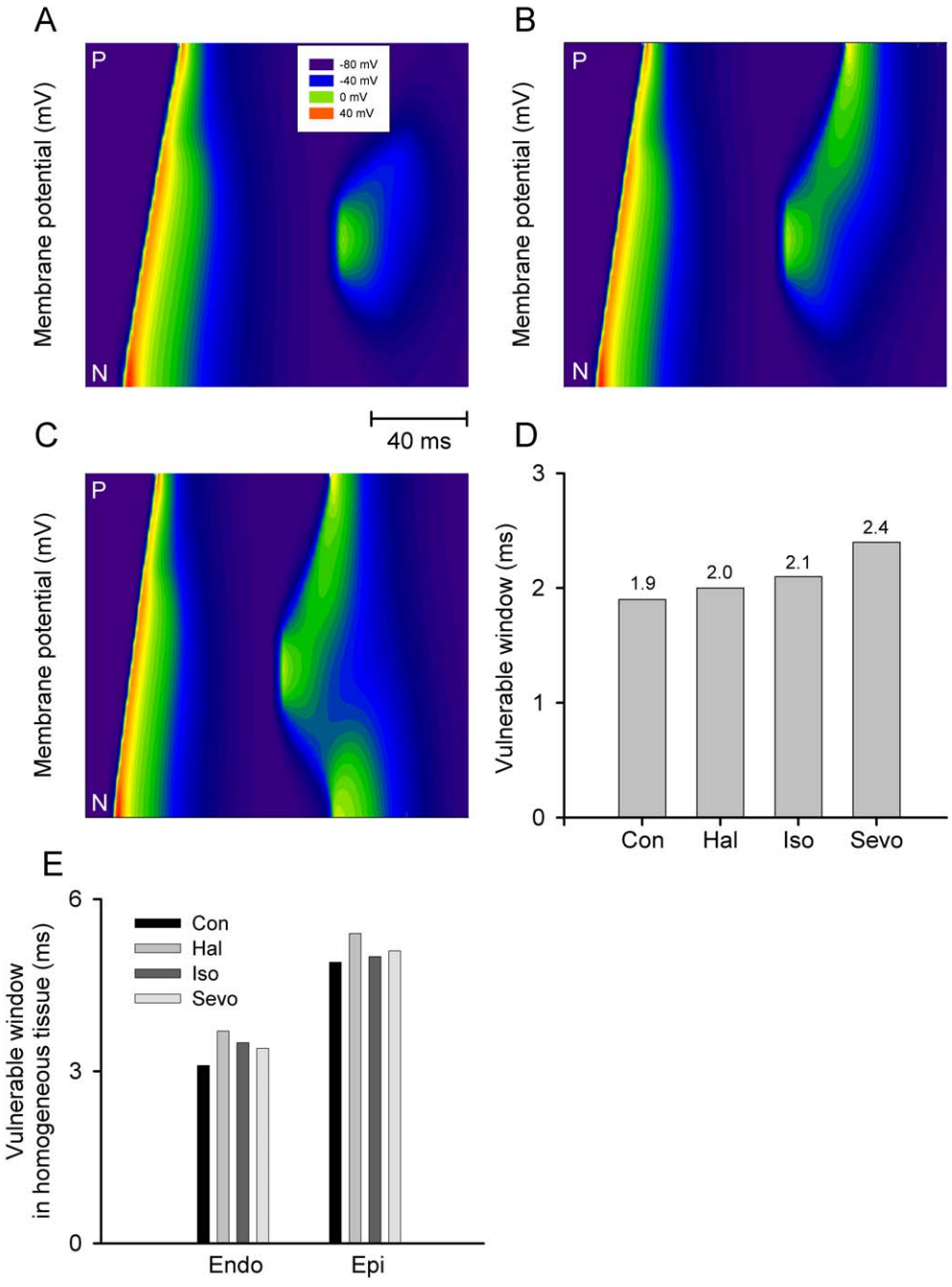

FIg 4

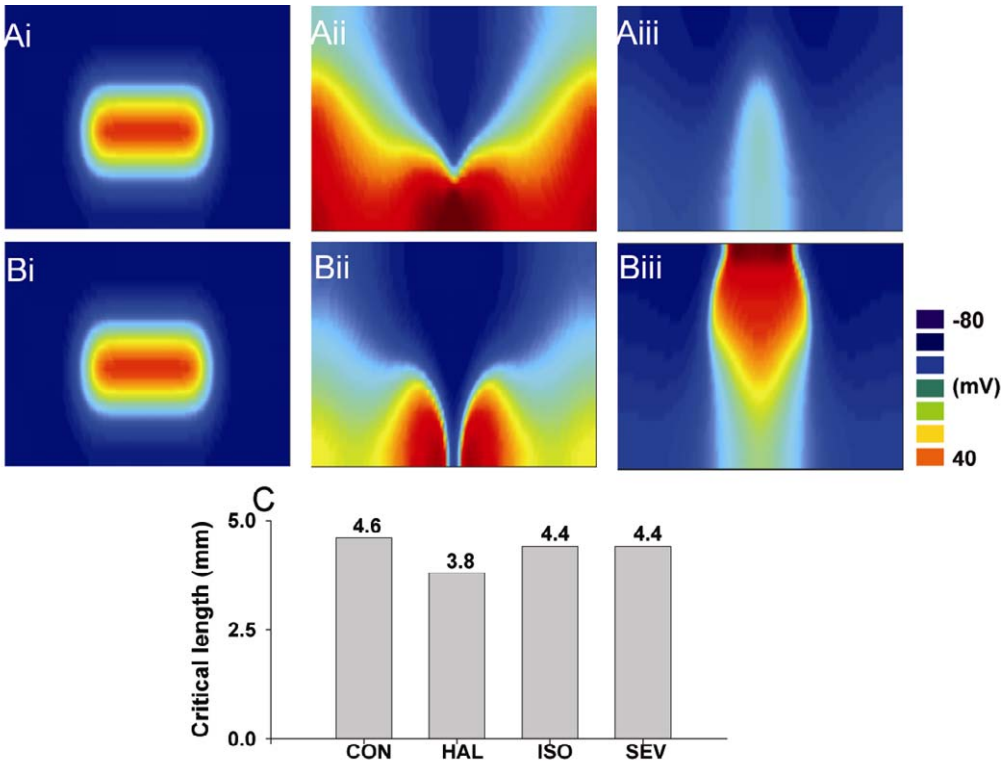

Figure 4

FIg 5